

Structure design for high performance n-type polymer thermoelectric materials

Qi Zhang(张奇), Hengda Sun(孙恒达), and Meifang Zhu(朱美芳)

Citation: Chin. Phys. B, 2022, 31 (**2**): 028506. DOI: 10.1088/1674-1056/ac3a64
Journal homepage: http://cpb.iphy.ac.cn; http://iopscience.iop.org/cpb

What follows is a list of articles you may be interested in

N-type core-shell heterostructured Bi_2S_3@Bi nanorods/polyaniline hybrids for stretchable thermoelectric generator

Lu Yang(杨璐), Chenghao Liu(刘程浩), Yalong Wang(王亚龙), Pengcheng Zhu(朱鹏程),Yao Wang(王瑶), and Yuan Deng(邓元)
Chin. Phys. B, 2022, 31 (**2**): 028204. DOI: 10.1088/1674-1056/ac272e

Thermal resistance matrix representation of thermal effects and thermal design of microwave power HBTs with two-dimensional array layout

Rui Chen(陈蕊), Dong-Yue Jin(金冬月), Wan-Rong Zhang(张万荣), Li-Fan Wang(王利凡), Bin Guo(郭斌), Hu Chen(陈虎), Ling-Han Yin(殷凌寒), Xiao-Xue Jia(贾晓雪)
Chin. Phys. B, 2019, 28 (**9**): 098502. DOI: 10.1088/1674-1056/ab3436

Highly sensitive polymer photodetectors with a wide spectral response range

Mile Gao(高米勒), Wenbin Wang(王文斌), Lingliang Li(李凌亮), Jianli Miao(苗建利), Fujun Zhang(张福俊)
Chin. Phys. B, 2017, 26 (**1**): 018201. DOI: 10.1088/1674-1056/26/1/018201

In-situ characterization of electrochromism based on ITO/PEDOT:PSS towards preparation of high performance device

Xue-Jin Wang(王学进), Zheng-Fei Guo(郭正飞), Jing-Yu Qu(曲婧毓),Kun Pan(潘坤), Zheng Qi(祁铮), Hong Li(李泓)
Chin. Phys. B, 2016, 25 (**2**): 028201. DOI: 10.1088/1674-1056/25/2/028201

TOPICAL REVIEW — Organic and hybrid thermoelectrics

Structure design for high performance n-type polymer thermoelectric materials

Qi Zhang(张奇), Hengda Sun(孙恒达)†, and Meifang Zhu(朱美芳)

State Key Laboratory for Modification of Chemical Fibers and Polymer Materials, College of Materials Science and Engineering, Donghua University, Shanghai 201620, *China*

(Received 24 August 2021; revised manuscript received 5 November 2021; accepted manuscript online 17 November 2021)

Organic thermoelectric (OTE) materials have been regarded as a potential candidate to harvest waste heat from complex, low temperature surfaces of objects and convert it into electricity. Recently, n-type conjugated polymers as organic thermoelectric materials have aroused intensive research in order to improve their performance to match up with their p-type counterpart. In this review, we discuss aspects that affect the performance of n-type OTEs, and further focus on the effect of planarity of backbone on the doping efficiency and eventually the TE performance. We then summarize strategies such as implementing rigid n-type polymer backbone or modifying conventional polymer building blocks for more planar conformation. In the outlook part, we conclude forementioned devotions and point out new possibility that may promote the future development of this field.

Keywords: organic thermoelectrics, conducting polymers, organic semiconductor doping

PACS: 85.80.Fi, 82.35.Cd, 81.05.Fb **DOI:** 10.1088/1674-1056/ac3a64

1. Introduction

With the rapid development of soft electronics during recent decades, wearable and flexible smart electronic devices have bloomed and significantly improved people's daily life. Some predictions forecast that the market value of wearable smart devices may grow to over 50 billion US dollars in the next few years.[1] However, conventional batteries failed to meet newly emerged requirements in these fields, for their hard shape, frequent charge/discharge and short life are fatal disadvantageous. Therefore, durable, flexible and self-charging power sources may boost the implement of wearable smart devices.[2–6] Thermoelectric materials can convert temperature gradient into electricity (Seebeck effect), and vice versa (Peltier effect), which makes them very useful in self-power wearable applications when harvesting body heat, or as heat management modules when electrified. Conventional thermoelectric materials are mostly inorganic ceramics, such as PbTe, SnSe, SiGe, *et al.*[7] However, these rigid materials fail to meet the requirement of being easily flexible for practical use in wearable devices. On the other hand, inorganic thermoelectric materials can only operate efficiently within high temperature window,[8] which is much higher than human's body temperature. Therefore, organic thermoelectrics (OTEs) with the advantages of being intrinsically flexible and operating under room temperature have drawn researchers' attention in recent years.[9] Unlike their inorganic counterparts, organic thermoelectrics utilize mostly conjugated polymers that are intrinsic highly flexible and deformable, which enable them to attach adequately to surfaces with complex interfaces such as human's wrist and knees.[10–13] Moreover, compared to inorganic thermoelectric materials that can only be fabricated into devices with large volume and heavy weight, organic thermoelectric materials are lightweight and can be fabricated into thin films or fibers to further increase flexibility, which bring comfortable wearing experience of wearable devices.

Seeking for commercial applications, OTEs are often fabricated into the two-leg p–n complementary structures, as shown in Fig. 1(b). To achieve a high performance OTE, adequate and matched performances of p- and n-type legs are prerequisites. However, to date, the performance of n-type organic thermoelectric materials is lagging far behind that of p-type ones, mostly because of the low doping efficiency, accordingly inferior electrical conductivity.[14] By the difference of component, n-type OTEs can be fabricated by n-type conjugated polymers or their derivatives, metal-coordination polymers,[15,16] polymer composites[17,18] or small molecules.[19,20] Recently, improving the thermoelectric performance of n-type conjugated polymers has been the point of research interest. In this mini review, we are going to briefly exam the working principles of OTEs, check the key points of building high performance n-type OTEs, and how to achieve that from the viewpoint of polymer structure design, especially backbone planarity.

†Corresponding author. E-mail: sunhengda@dhu.edu.cn

© 2022 Chinese Physical Society and IOP Publishing Ltd

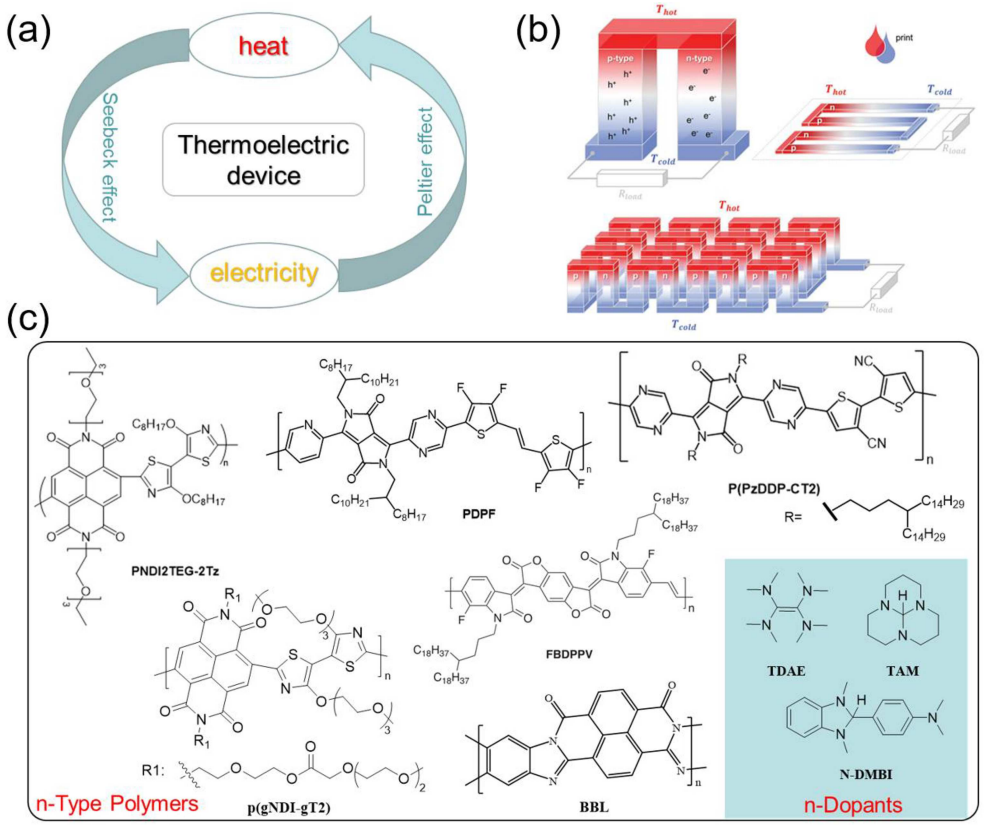


Fig. 1. (a) Thermoelectric effects. (b) Structure schematic of a typical thermoelectric element and the printed thermoelectric generator,[21] adapted with permission, copyright 2016 The Royal Society of Chemistry. (c) Examples of some reported high performance n-type thermoelectric polymers and n-dopants.

2. Working principles of OTE

Thermo-voltages occur when a conductor or semiconductor is put in an environment with temperature gradient, which will inspire charge carriers diffuse from high temperature side to low temperature side thus create a potential difference. Seebeck coefficient is the measurement of thermo-voltage generated per temperature unit $\alpha = -\Delta V/\Delta T$, α can be positive or negative, which is an indicator to define the type of polymer semiconductor. In most cases, positive α suggests that the polymer is a p-type semiconductor transporting holes, while a negative α is a sign of n-type semiconductor transporting electrons, with some exceptions.[22] Though the altitude of Seebeck coefficient is critical to a thermoelectric polymer, electrical conductivity also plays an important role in determining the comprehensive thermoelectric performance. By focusing evenly on the α, the thermal conductivity κ, the electrical conductivity σ, after setting an ideal test environment which gets ward off the affection of heat lose, the figure-of-merit value ZT is used to evaluate the overall performance of a thermoelectric material:

$$ZT = \frac{\alpha^2\sigma}{\kappa}T.$$

Thermo-conductivity is challenging to measure precisely in many kinds or shapes of materials, especially in organic thermoelectric thin film devices.[23,24] In many cases, the power factor $PF = \alpha^2\sigma$ is also widely used instead as a similar indicator. A typical inorganic thermoelectrical material shows a $ZT > 1$, while recent p-doped OTE has just exceed 0.4 and n-doped OTE is still suffering from much inferior ZT value.[9] To improve the performance of n-type devices to match that of p-type ones is currently the key issue for OTE research and applications. Because a practical thermoelectric convertor consists of two legs made individually from p- and n-type thermoelectrical materials, as displayed in Fig. 1(b). Although single carrier type (n- or p-) leg devices can be constructed, connecting alternating n- and p-type legs electrically in series (and thermally in parallel) enables more efficient interconnects, decreasing parasitic thermal leakages and allowing the maximum power generation from a heat source.[9]

A desired OTE device should possess high α, high σ and low κ. However, the three parameters are rather coupled together. Usually an increased σ is accompanied by a decreased α but increased κ, as the electronic part of κ (where $\kappa = \kappa_{\text{phonon}} + \kappa_{\text{electronic}}$) is proportional to the rate of carrier transport. Therefore, to find a balance in compromising the the three parameters is critical to OTE performance, which indeed can be done effectively by the practice of doping. Doping is to deliberately add dopant molecules into the pristine matrix, triggering charge transfers between the two to release mobile holes (p-doping) or electrons (n-doping) into the system. Orders of magnitudes higher σ could be achieved upon efficient doping.[25,26] In organic semiconductors doped to dif-

ferent levels, the σ may reach well over 1000 S/cm for p-type materials, but struggling to reach 100 S/cm for n-type materials.[27,28]

Currently, various types of conductive polymers with thermoelectric properties have been put into research and practical use. Efforts are mainly focused on two key aspects: (1) to modify the processing strategies for easier and cheaper ways and more suitable for large yield, (2) to discover novel polymers and dopants to achieve higher performance, such as high output, high durability, as well as low toxic process and raw materials. After decades of devotions, several kinds of polymers have been established, typical p-type polymers includes containpolythiophene (PBTTT), polyaniline (PANI), poly(3,4-ethylenedioxythiophene) (PEDOT), polyacetylene (PA), *et al.*,[29–32] with tosylate (Tos), poly(styrenesulfonate) (PSS), camphorsulfonic acid (CSA) and some Lewis acids often used as p-dopants. Typical n-type polymers include copolymers or derivatives from perylene diimide (PDI), naphthalene diimide (NDI), bithiopheneimide (BTI), naphthodithiophenediimide (NDTI), p-phenylene vinylene (PPV), poly(benzimidazobenzophenanthroline) (BBL), *et al.*[9,33–35] The choices of charge carrier providing dopants are limited, most of them are based on N-DMBI, TDAE or TAM.

Table 1. Thermoelectric performance of some n-type TE polymers.

Polymer	Dopant	Processing method	σ (S/cm)	α (μV/K)	$\alpha^2\sigma$ (μW·m^{-1}·K^{-2})	Ref.
P(NDI2OD-T2)	N-DMBI	solution mixing	8×10^{-3}	−850	0.6	[36]
P(NDI2OD-T2)	TDAE	vapor doping	3×10^{-3}	−200	0.012	[35]
P(NDI2OD-Tz2)	TDAE	vapor doping	0.09	−447	1.5	[37]
P(NDI2TEG-2Tz)	N-DMBI	solution mixing	1.36	167	3.8	[38]
P(NDI2C8TEG-2Tz)	N-DMBI	solution mixing	1.6	326	16.5	[38]
BDPPV	N-DMBI	solution mixing	0.26	−320	1.6	[39]
CIBDPPV	N-DMBI	solution mixing	7	−220	16.5	[39]
FBDPPV	N-DMBI	solution mixing	14	−210	25.5	[39]
FBDPPV	(N-DMBI)$_2$	solution mixing	8	150	7	[40]
FBDPPV	DMImC	solution mixing	7	182	16	[41]
LPPV-1	TAM	solution mixing	3.7	204	33.9	[42]
UFBDPPV	TAM	solution mixing	22.5	198	8	[42]
TBDPPV	N-DMBI-H/(RuCp*mes)$_2$	solution mixing	85	/	76	[43]
TBDOPV-T	N-DMBI-H/(RuCp*mes)$_2$	solution mixing	59	/	106	[43]
BBL	TDAE	vapor doping	2.4	−40	0.43	[35]
BBL	N-DMBI	sequential casting	1.1	−212	1.5	[34]
P(PymPh)	NaNap	immersing	18	−16.4	0.49	[44]

3. Towards high performance n-type OTE

The large gap in conductivity between the p-type and n-type thermoelectric materials has prevented further development in OTE. Gradually, such dilemma of n-type thermoelectric materials can be attributed to several reasons, partly concluded by Pei *et al.*:[14] 1) the efficiency of n-doping is inadequate, which results in uneven and insufficient interchain charge transport. 2) The miscibility of dopant and n-type polymer is a critical issue that remains to be solved, the poor miscibility leads to uneven dopant and eventually eliminates the improvement of conductivity. 3) The intrachain charge movement is also limited by the low mobility of charge carriers. 4) Mostly, the doped n-type materials can only be stably operated and kept under nitrogen atmosphere, when put in air, the diffusion and escaping of charge carrying and transporting organic anions will soon deteriorate and quench. Such poor air stability restricts their applications in practical circumstances.

Researchers have devoted in solving these disadvantageous. Since the critical fact that determines the stability of n-type polymers is their high LUMO level, lowering the LUMO level turns to be a useful strategy.[45] A LUMO level which is adequate low that can help n-type polymers remain their properties during operation, though it is extremely challenging to achieve. Besides, it is also a proper way to enhance the doping quality by improving hydride transfer, or adding electron-deficient function groups onto the backbone of n-type polymers. Lei *et al.* synthesized a novel pyrazine-flanked diketopyrrolopyrrole (DPP) based polymer,[46] with the lowest LUMO level among all reported DPP derivatives. Doped with N-DMBI, the synthesized P(PzDPP-CT2) was estimated to have LUMO level about −4.03 eV, much lower than P(TDPP-CT2) with −3.70 eV. Moreover, hydrogen bonds were found between the pyrazine and DPP, further improving the spatial structure of the polymer chain. The conductivity of P(PzDPP-CT2) could reach 8.4 S/cm after doping, while P(TDPP-CT2) was merely 0.39 S/cm. The P(PzDPP-CT2) also exhibited 57.3 μW·m^{-1}·K^{-2} in PF, which was over 5 times higher than that of P(TDPP-CT2).

Conventional n-doped materials often suffer from phase segregation at high doping level and lead to the formation of discontinuous charge carrier pathways, thus dramatically decrease the overall conductivity. Mostly, such flaw is often attributed to the strong donor–acceptor interaction ability, to reduce the affection of this issue, several strategies have

been concluded. In general, the main idea is to modify the chain to be more polarized or twisted in spatial structure, thus regulate the interactions among polymer chains and dopants. Based on the most widely studied NDI polymer, Muller *et al.* introduced copolymer with polar side chains with high conductivity and good miscibility.[47] By branching NDI with bithiophene (gT2), another well-known polar donor motif, the synthesized p(gNDI-gT2) possessed similar structure with p(NDI2OD-T2). While the p(NDI2OD-T2) was hard to mix well with N-DMBI dopant, often resulting dopant aggregation on surface, the N-DMBI doped p(gNDI-gT2) exhibited superior miscibility even in a high doping level as 20 mol%. By employing atomic force microscopy (AFM), scanning electron microscopy (SEM) and grazing-incidence wide-angle scattering (GIWAXS), researchers found that though there were also aggregation of dopant on the surface, it seemed to have little affection on the polymer nanostructure. Moreover, the polar side chain successfully prevented N-DMBI from aggregating, enhancing the conductive chain length and miscibility. Only over 20 mol% that the dopant started to show a few aggregated groups.

In another work, Pei group reported superior miscibility of n-type polymers and the dopant in solution based process with record high conductivity.[27] The polymer chain consisted of thiophene fused benzodifurandione-based oligo (p-phenylenevinylene) (TBDOPV) and polymerized with different linking units, trans-vinylene (TBDPPV), 2,5-thienylene (TBDOPV-T) or 2,2′-bithiophene-5,5′-diyl (TBDOPV-2T). The co-polymer was then co-deposited with N-DMBI or $[RuCp^*mes]_2$, molecule structures shown in Fig. 2(a). With ordered chain and disordered microstructure, the TBDPPV polymer was estimated to achieve highest conductivity about 85 ± 7 S/cm (Fig. 2(b)), which was considered to be the contribution of effective and high doping level. In the GIWAXS test, it was found that the TBDPPV was highly tolerative to dopant in different percent levels, the stacking distance almost remained the same even when the doping level came up to 50 mol%, as illustrated in Fig. 2(c). Normally, such high content would result in obvious dopant aggregation, but a hypothesis was put out thought the reduction of lamellar order by using short conjugated linking motifs could keep the stacking distance and planarity while accommodate dopants in the largest extent.

On the other hand, a better miscibility can not only be gained by modifying the polymer matrix, the implement of novel dopants is also feasible ways. As a widely used n-type dopant, benzimidazole derivative monomers have proved its reliability and high performance. Most of such derivatives are based on N-DMBI. However, this group of derivatives suffer from the requirement of high HOMO to match with n-type polymers. Moreover, they are vulnerable to air and water, which restrict the durability of devices. Tailoring the chemical construction of N-DMBI is a reasonable strategy to enhance miscibility, stability and other properties. Comparing dimerized $(N\text{-DMBI})_2$, N-DMBI-H and $N\text{-DMBI}^+$ and some other

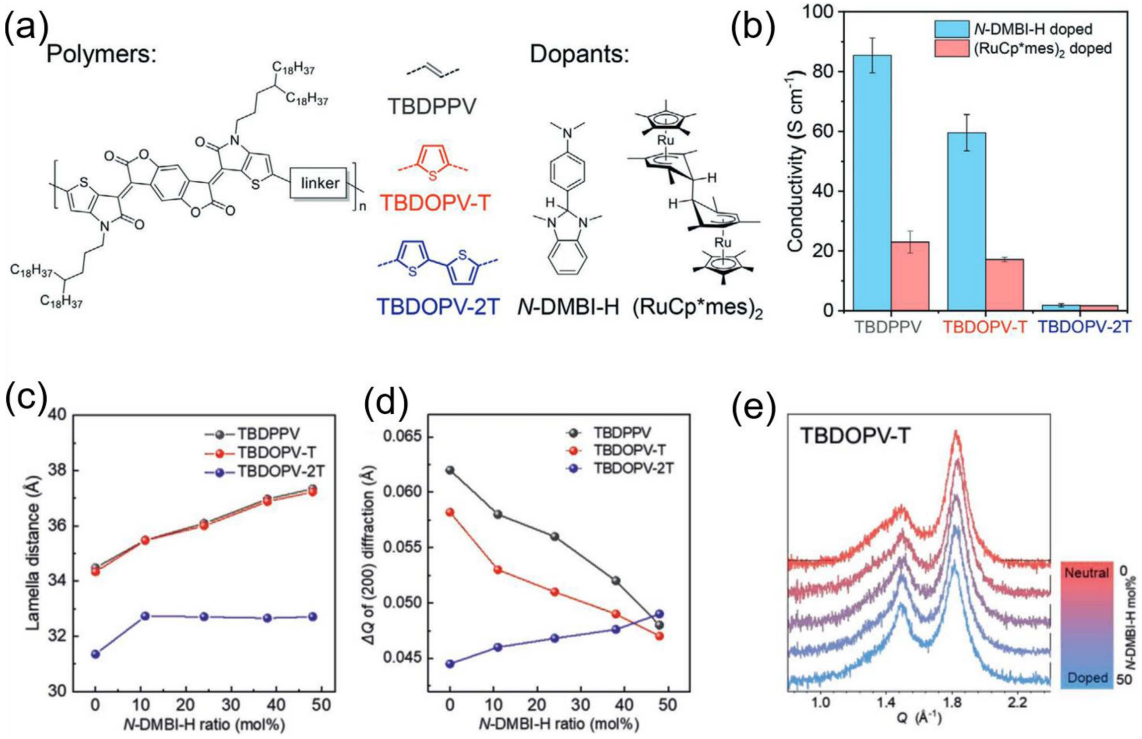


Fig. 2. A high miscibility n-type polymer example.[27] (a) Chemical structures of the three conjugated polymers and the two n-dopants used. (b) Maximum values of electrical conductivities obtained for N-DMBI-H- and $(RuCp^*mes)_2$-doped polymers. (c) Lamellar distance of the (200) peak position and (d) linewidth of the (200) peak for thick films. (f) 1D-GIWAXS linecuts of TBDOPV-T at different dopant (N-DMBI-H) ratios (out-of-plane direction), showing the π-stacking (010) peak at $Q \approx 1.8$ Å^{-1}. Adapted with permission, copyright 2020 Wiley-VCH GmbH.

dopants, Pei and others discussed the difference of doping resulted from chemical structure modification.[40] To understand the structure induced performance variations, a novel dimer based on conventional N-DMBI was synthesized, this $(N\text{-}DMBI)_2$ was doped with FBDPPV, with $(RuCp^*mes)_2$ and N-DMBI-H chosen as comparison counterparts. Spectra patterns of UV-vis-NIR revealed that dimer type dopants could grant higher doping efficiency by providing double electron transfer. Higher polaronic variations were also observed in $(RuCp^*mes)_2$ and $(N\text{-}DMBI)_2$ doped FBDPPV. To achieve similar thermoelectric performances, the quantity of N-DMBI-H needed to be double of the dimer type $(N\text{-}DMBI)_2$, suggesting the difference in doping efficiency. The eventual performances of $(N\text{-}DMBI)_2$ were superior to $(RuCp^*mes)_2$. In AFM and GIWAXS scans, the smaller dopant size and more planar side chains of N-DMBI derivatives were investigated to put less affection on polymer morphology, while the π–π stacking distance remained almost the same in two N-DMBIs, but it seemed the bulky $(RuCp^*mes)_2$ has resulted in a disturbed π–π interaction and larger lamellar distance. Combined with the results of AFM and scanning Kelvin probe microscopy (SKPM), when the doping levels were competitive (46 mol% of $(RuCp^*mes)_2$ and 43 mol% of $(N\text{-}DMBI)_2$), the lamellar distance of $(RuCp^*mes)_2$ was larger and much rougher, as well as a failure in calculating π–π stocking distance. These outcomes suggested that a designed effective dopant with smaller and more planar structure could help achieving high thermoelectric performance.

Among all the afore mentioned features that can affect conductivity, the aggregation structure of the conjugated backbone is the most determinative. Many decreases in conductivity can be regarded as the contribution of destroyed planar backbone stacking. These backbone stacks allow charge carriers to delocalize among different polymer chains, thus to promote electron conduction. This process is amplified by n-doping so that enough mobile carriers can be released into the polymer matrix which can eventually have sufficient conductivity for practical uses. The occurrence of polarons and bipolarons is the key to understand the physical mechanism of this process. When doped effectively by n-type dopants, charge transfer among dopant and polymer backbone will lead lattices of the polymer to be distorted, the excess electrons may be delocalized along the backbone, and a polaron is created. As the doping level increases, the band gaps will come closer and enlarge in width, activating more electrons to be delocalized, the wave functions in neighbor or same backbones will partially lap over each other, this more activated delocalization is called bipolaron state. Since only effective doping can enhance the properties of thermoelectric devices, too high doping level may do harm to eventual conductivity by destroying stacking condition and forming dopant aggregation, a proper doping level with patterned and fine stacked polymer backbones will maximum the conductivity.

4. Significance of rigid and planar backbone

As mentioned before, a planar backbone structure may optimize the π–π stacking thus increase the polaron interchain delocalization. In conventional n-type backbones, mostly the repeating units are connected by single-bond, leaving a certain level of dihedral rotational freedom, which may hinder the delocalization of polarons after doping. In 2016, Fabiano group introduced a novel n-type polymer poly(benzimidazobenzophenanthroline) (BBL) with ladder structure backbone.[35] By implementing double-bond to form conjugated chains, they successfully achieved a torsion-free planar polymer backbone in homopolymer. Doped with TDAE, a strong reductive agent, its conductivity could reach a high value of 2.4 S/cm (Fig. 3(c)). BBL is not a donor–acceptor polymer like P(NDI2OD-T2) in this article as counterpart, and contributed by extremely rigid aromatic rings and double-bonds on backbones, it also possesses higher thermal stability and high glass transition temperature. Moreover, many rigid n-type polymer thermoelectrical materials may suffer from poor processibility, while BBL can be fabricated by solution process, which grants it large feasibility in future massive printing manufacture. Combining these advantages, BBL appears to be an outstanding potential candidate for high performance n-type OTEs. The conductivity of pristine BBL was about 10^{-7} S/cm, after exposed in TDAE vapor with various time from several seconds to over 20 hours, the after-doped conductivity first raised to a maximum parameter of about 2 S/cm, then slightly dropped down to lower degree and finally remained stable, suggested great resistance to over doping, compared to other D-A type polymers. An extra durability test then elucidated that the doped BBL could maintain the electrical conductivity after kept in nitrogen atmosphere after several weeks. In UV-vis-NIR spectra testes aided with TD(DFT) calculations, compared with pristine BBL, appearance of a new band at about 900 nm was observed (Fig. 3(b)), which was ascribed to the affection of doping induced polaron transition. When the doping level ascended, the experimental trend of strengthening polaronic effect was agreed to the calculated results. Benefitted from the planar spatial conformation, the spin densities on BBL and P(NDI2OD-T2) oligomer chains were investigated, a three-units length delocalization of polaron on BBL was assumed, while there was merely one unit in length on P(NDI2OD-T2), as shown in Fig. 3(a), suggesting that the planar structure induced polaron transport was superior to donor–accepter character, further the conductivity. Since the BBL can retain the ordered and planar structure in a long range, these delocalized charge carriers can easily travel through the

backbone, giving lower Arrhenius activation energy to BBL than P(NDI2OD-T2), 0.12 eV and 0.28 eV, respectively. GI-WAXS and TEM were applied to scan the morphology of the doped polymer. The before and after doping P(NDI2OD-T2) exhibited an obvious disappearance of face-on orientation, the (010) peak smoothness implied a degradation of π–π stacking. The BBL samples underwent a substantial change while being doped in different levels. From all the scattering outcomes, both pristine and doped BBL possessed best π stacking structure and order. After fabricated into thin films, the Seebeck coefficients of BBL and P(NDI2OD-T2) were tested, underwent a reverse trend to conductivity change upon doping, the best Seebeck coefficient and conductivity occurred respectively as -400 ± 25 μV/K and 1.7 S/cm. When came to the highest σ, the Seebeck coefficient decreased to -60 ± 4 μV/K. For comparison, the Seebeck coefficient of P(NDI2OD-T2) varied from -790 ± 14 μV/K to -150 ± 5 μV/K when σ raise from 1×10^{-4} S/cm to 3×10^{-3} S/cm (Fig. 3(e)). Interestingly, the thermal variation affected the performance of doped P(NDI2OD-T2) largely due to the more flexible microstructure. Another critical index, power factor, BBL with 0.43 $\mu W \cdot m^{-1} \cdot K^{-2}$ in maximum was more than one order of magnitude higher than 0.013 $\mu W \cdot m^{-1} \cdot K^{-2}$ of P(NDI2OD-T2). This research demonstrated that a rigid planar backbone structure polymer is superior to traditional D-A polymers in doping efficient and electrical conductivity. Several further researches including modifying BBL backbone, computational simulation to understand its mechanism and comparing BBL made devices to other counterparts, were reported.[48]

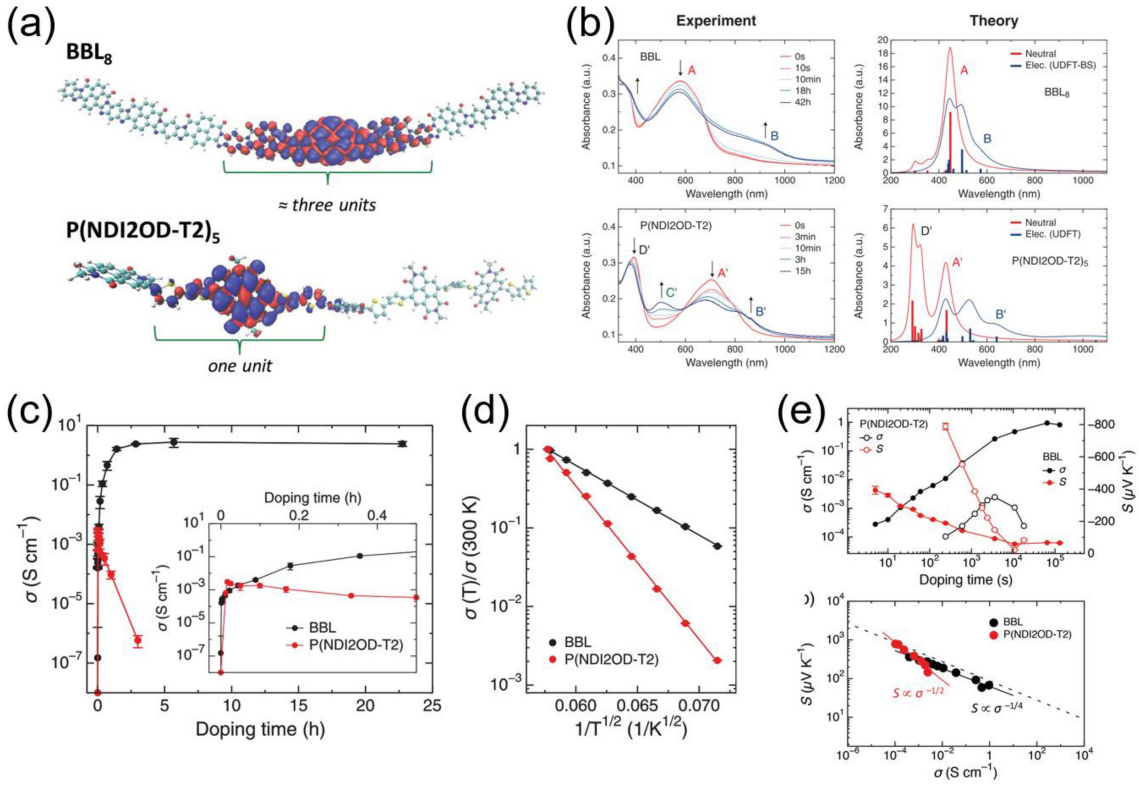


Fig. 3. The example of rigid n-type ladder polymer BBL.[35] (a) Spin (α and β) density distributions of the longest BBL ($n = 8$, top) and P(NDI2OD-T2) ($n = 5$, bottom) oligomers, as calculated at the UDFT-BS and UDFT levels, respectively. (b) Experimental (left) and calculated (right) UV–vis–NIR absorption spectra of BBL and P(NDI2OD-T2) films for different TDAE exposure times. (c) Electrical conductivity of BBL and P(NDI2OD-T2) films as a function of the TDAE exposure time (doping time) and (d) temperature dependence of the electrical conductivity (normalized to 300 K) for doped BBL and P(NDI2OD-T2) samples. (e) Electrical conductivity σ and Seebeck coefficient S versus TDAE doping time for BBL and P(NDI2OD-T2) films and Seebeck versus conductivity data for BBL and P(NDI2OD-T2). Adapted with permission, copyright 2016 WILEY-VCH Verlag GmbH & Co. KGaA, Weinheim.

Since tailoring the backbone of BBL is a tough work, researchers have turned their eyes onto different processing techniques of BBL in order to further enhance device properties. Reported again by Fabiano group, a sequential doping process allows BBL-made OTE appears to be more thermally stable.[34] The widely used N-DMBI was choose to be the dopant, the thin film device was prepared by dynamically drop N-DMBI solution onto dried BBL film while spinning. In following examinations, this sequential doped BBL showed highest electrical conductivity when it was annealed at 210 °C, reached about 1.1 ± 0.3 S/cm, which was similar to previously reported TDAE doped BBL. The Seebeck coefficients of doped BBL reduced monotonically while the annealing temperature increased, dropped from -212 ± 20 μV/K to -112 ± 14 μV/K while the temperature raised from 70 °C to 210 °C. The best power factor occurred when the annealing temperature was 190 °C, reaching to 1.5 ± 0.3 $\mu W \cdot m^{-1} \cdot K^{-2}$. Notably, this sequential N-DMBI doped BBL possessed out-

standing thermal stability, after heated at 190 °C for 20 h, the properties of the film remained the same, which indicated that such material was heavy-duty. Cooperated by EPR analysis, optical absorption spectroscopy and vibrational spectroscopy characterization, it was found that the increasing trend of charge carrier density was agreed to the change of polaronic property, though it kept raising after 210 °C while the occurrence of dopant loss because of energetic disorder at high temperature. Moreover, in GIWAXS, a slight increase of π–π stacking of doped BBL was observed. These outcomes suggested that obtaining good polaronic property is the key to gain high performance n-type polymer.

PPV is another potential candidate with rigid coplanar backbone. Lu *et al.* synthesized two PPV derivatives (structure schematic in Fig. 4(a)), LPPV-1 and LPPV-2, with difference in the side function group.[49] The PPVs are connected by carbon double bonds, which grants them stiffness and almost planar backbone structure with a merely 2.7° torsion angel between the two blocks (Fig. 4(b)). Four highly electron-drawing carbonyl function groups provided PPV with low LUMO as −4.49 eV. These specialties offered PPV and its derivates longer charge carrier delocalization length up to 6 units on the polymer chain. The air stability was tested to be over a week. When possessing similar molecular weight and dispersity index, PPV-1 with smaller-R alkyl function group was superior to LPPV-2 with larger-R function group. In GIWAXS measurement, LPPV-1 exhibited closer π–π stacking. Processed into thin film OTE devices, LPPV-1 exhibited 1.1 S/cm and 1.96 $\mu W \cdot m^{-1} \cdot K^{-2}$ in conductivity and power factor, respectively (Figs. 4(c) and 4(d)), which was among the highest solution processed n-type polymers. Since the electron mobility of LPPV-1 was one-fold higher than that of LPPV-2 while both of them possessed similar polaron density, the intrinsic electron mobility was considered to be a critical fact that determined the eventual performances, while such difference could be gained by regulating the monomer structure. Moreover, the air stability of LPPV-1 was observed as a merely 2% deterioration in performance after exposed in air for a week (Figs. 4(e) and 4(f)). In conclusion, the rigid backbone structure, combining the deep LUMO level induced by electron-deficient building blocks, leads the LPPV-1 to be a highly conductive and stable n-type thermoelectric polymer.

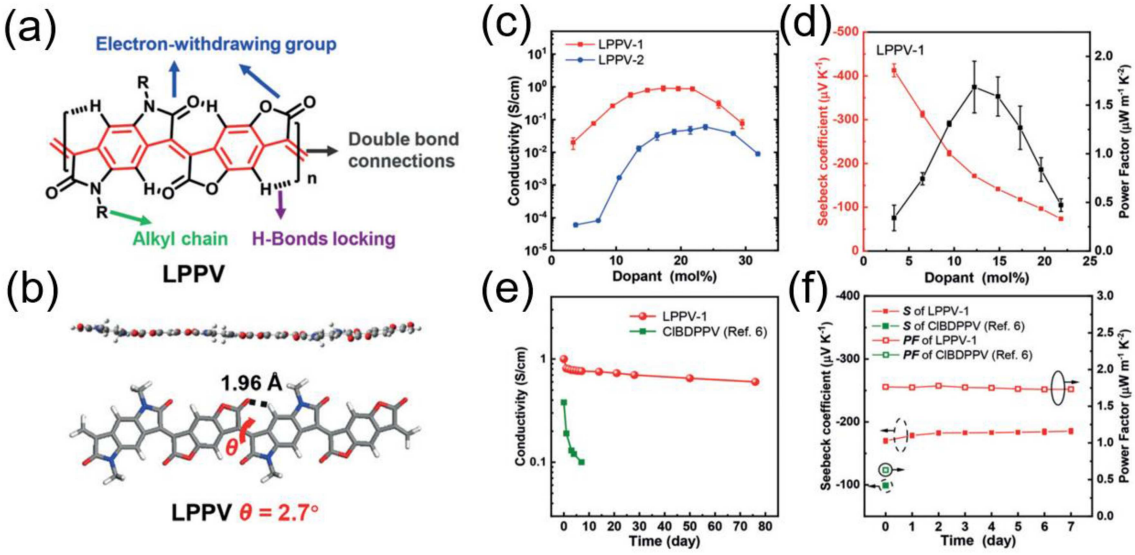


Fig. 4. PPV derivatives as rigid coplanar backbone n-type polymer.[49] (a) Rigid coplanar PPV derivative, LPPV structure; (b) DFT optimized geometries of LPPV. (c) Conductivity of the doped polymers at different concentrations of the dopant N-DMBI. (d) Seebeck coefficients and power factors of LPPV-1 for different dopant ratios. (e) Conductivity stability of the doped LPPV- 1 film in air in comparison to that reported TBAF-doped ClBDPPV. (f) Seebeck coefficient and power factor stability of the doped LPPV- 1 film in air under humidity of 50%–60%, and temperature of 298 K. Adapted with permission, copyright 2019 Wiley-VCH Verlag GmbH &Co. KGaA, Weinheim.

5. Molecular design for more planar backbone

Though the ladder-shape backbone structure grants BBL and other polymers outstanding thermoelectric performance, the issue of processibility remains to be critical. Most of these polymers are hard to be produced by common organic solution process but strong organic acids, which is fatal to environmental protection and industrial production. However, the idea of more planar and rigid backbone promoting n-type thermoelectric performance could be applied to extended material systems.

By modifying the conventional widely used n-type polymer P(NDI2OD-T2), a novel NDI2OD based polymer was synthesized and investigated by Fabiano and Marks group together.[50] By replacing bithiophene (T2) with bithiazole (Tz2), a function group with more electron-deficient ability, the strong D-A character is weakened, structures shown in Fig. 5(a), which thus enhances the eventually high electrical conductivity and power factor. Since higher molecular weight indicates longer polymer chain, which is beneficial to charge carrier mobility, active-zinc polymerization

is implemented.[51–53] The number-average molecular weight and dispersity of obtained P(NDI2OD-Tz2) are determined by gel permeation chromatography (GPC), which are 32.2 kDa and 1.7, respectively, suggesting relatively high molecular weight and narrow weight dispersity. Compared to tested data of P(NDI2OD-T2) in TGA and DSC, the melting and crystallizing temperatures of P(NDI2OD-Tz2) rise by 16 °C and 24 °C, respectively, exhibiting better intermolecular connection. These two polymers also possess different LUMO and HOMO levels, the LUMO level of P(NDI2OD-Tz2) is −4.10 eV while P(NDI2OD-T2) is −3.99 eV, the HOMO level of P(NDI2OD-Tz2) is −5.90 eV, lower than −5.46 eV of P(NDI2OD-T2). Such outcomes suggest potentially higher stability in ambient atmosphere and a reduced D-A characteristics for P(NDI2OD-Tz2). Further investigation of conformational and aggregational structures of P(NDI2OD-Tz2) was also explored. By aiding with density functional theory (DFT) calculation of co-planar conformations at 0° and 180° (Fig. 5(b)), it is obvious that P(NDI2OD-Tz2) can be better planarized by –Tz2 function groups branched onto the backbones than P(NDI2OD-T2), inducing stronger interactions among molecules. The calculation result in 180° indicates a more popular quasi-planar conformation at room temperature. After fabricated into organic field effect transistors (OFETs), both P(NDI2OD-T2) and P(NDI2OD-Tz2) show competitive electron mobilities of 0.10 $cm^2 \cdot V^{-1} \cdot s^{-1}$ and 0.20 $cm^2 \cdot V^{-1} \cdot s^{-1}$, respectively. But after exposed in TDAE dopant for various times, the electrical conductivity of the two polymers shows dramatical changes and diverse performance. The pristine P(NDI2OD-Tz2) possesses merely 10^{-8} S/cm and warps to 0.07 ± 0.02 S/cm after doped with TDAE for a short time scale of 16 s, which is over 30 times higher than that of P(NDI2OD-T2) when doped to the highest conductivity (Fig. 5(c)). Quantitative EPR measurement results of the two polymers at their maximum conductivity suggest a lower work function of P(NDI2OD-Tz2) than that of P(NDI2OD-T2), the respect spin density is 8.65×10^{20} cm^{-3} and 2.46×10^{19} cm^{-3}. Since both of the polymers have similar LUMO, HOMO and electron mobility, it is reasonable to ascribe such difference to better doping efficiency that resulted from backbone structure variation. UV-nis-NIR and GIWAXS patterns show stronger π–π stacking effect and closer interchain distance, which are consistent with the formation of negative polarons. The Seebeck coefficient of P(NDI2OD-Tz2) drops from -732 ± 31 μV/K to −227 μV/K, while the power factor reaches the maximum of 1.5 $\mu W \cdot m^{-1} \cdot K^{-2}$ (Figs. 5(e) and 5(f)), which is over a hundred times higher than the highest power factor obtained by P(NDI2OD-T2). However, the TDAE will instantly deteriorated by air, which prevents the doped polymers from practical use. Then the P(NDI2OD-Tz2) is doped with another well known dopant DMBI and tested, for the poor miscibility of DMBI is also well known, the outcome of conductivity is much lower than that of TDAE doped P(NDI2OD-Tz2).

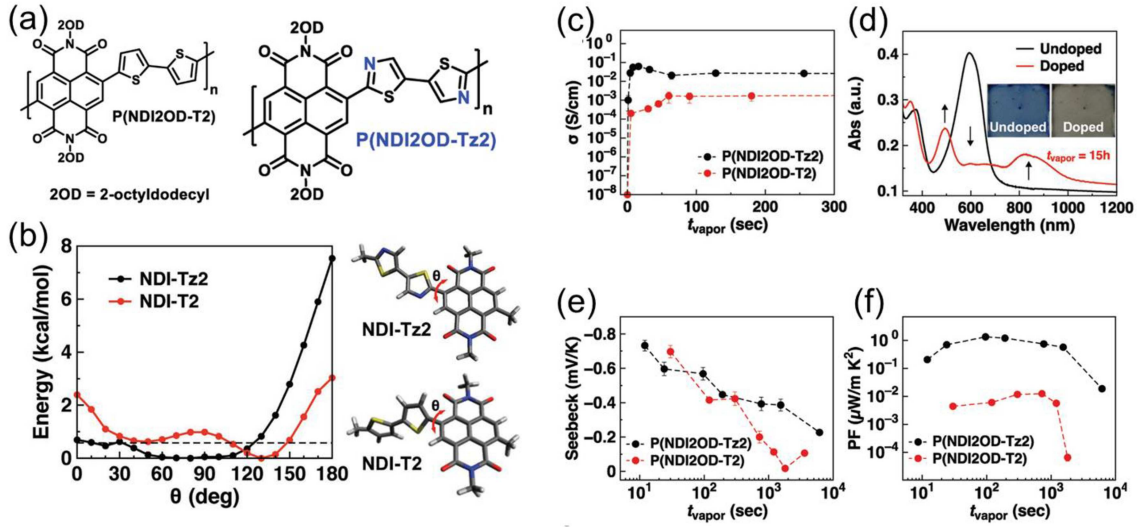


Fig. 5. Modifying the classic n-type polymer P(NDI2OD-T2) for a more planar backbone.[50] (a) Chemical structures of P(NDI2OD-T2) and P(NDI2OD-Tz2); (b) ωB97X-D/6-311G** relaxed potential energy–θ profiles for the indicated structures. The dashed line denotes $k_B T \approx 0.6$ kcal·mol^{-1} at 298 K. (c) Electrical conductivity of P(NDI2OD-Tz2) and P(NDI2OD-T2) films as a function of TDAE tvapor. (d) Optical absorption spectra (inset, optical images) of P(NDI2OD-Tz2) films before and after TDAE doping (t_{vapor} = 15 h). (e) Seebeck coefficient and (f) thermoelectric power factor (PF) as a function of TDAE exposure time for P(NDI2OD-Tz2) and P(NDI2OD-T2) films. Adapted with permission, copyright 2018 WILEY-VCH Verlag GmbH & Co. KGaA, Weinheim.

Others also utilized the concept of creating charge carrier mobile-friendly planar backbones. In another work, Liu *et al.* modified PNDI2TEG-2T repeating unit by replacing alkyl with ethylene glycol substituents, the dihedral angle was reduced from 40° to 1°, largely improved the planarity of the polymer backbone.[54] The electron rich bithiophene function group was replaced by electron donative bithiazole. The introduction of N atoms was ascribed to be the reason of more

planar structure. In GIWAXS measurement, beside the conventional reflection indicated a π–π stacking of NDI blocks, an extra peak at about 3.6 Å may related to the π–π stacking of the introduced bithiazoles. Doped with N-DMBI, the modified PNDI2TEG-2Tz exhibited 1.8 S/cm of conductivity when the dopant percentage was 21%. This result was 5 grades of magnitude higher than the best of PNDI2TEG-2T, which was observed when the dopant concentration was 42 mol%. Together with -159 ± 8 μV/K in Seebeck coefficient, the PF of PNDI2TEG-2Tz was calculated to be 4.6 ± 0.2 μW·m^{-1}·K^{-2}, tremendously higher than that of PNDI2TEG-2T. These outcomes proved that the strategy used to modify PNDI2TEG-2T was a success to regulate D-A characters.

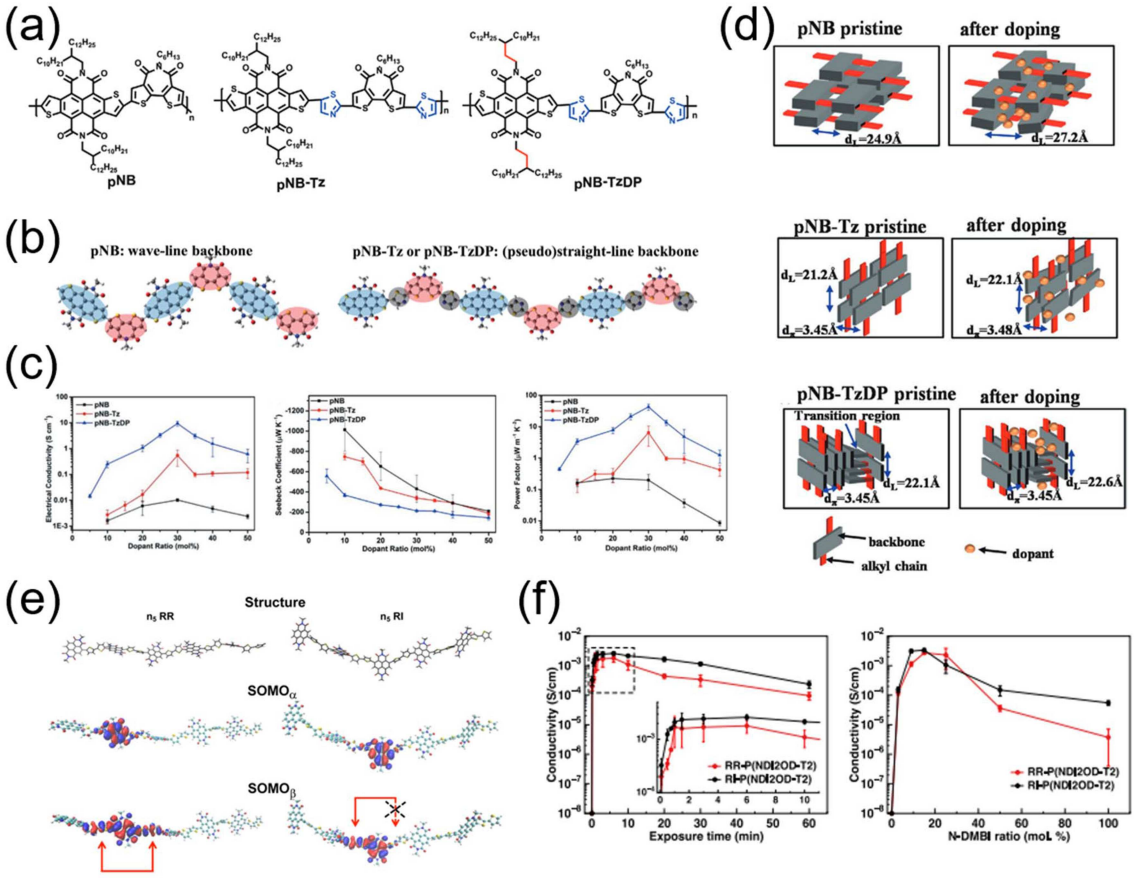


Fig. 6. Novel pNB based n-type thermoelectric polymers.[37] (a) Chemical structures of polymers pNB, pNB-Tz, and pNB-TzDP. (b) DFT calculation results of backbone geometry. (c) Dopant-ratio-dependent electrical conductivities, Seebeck coefficients and power factors of polymer films. (d) Cartoon representations of molecular packing of pNB, pNB-Tz, and pNB-TzDP polymer films before and after doping. Copyright 2020 The Authors. Published by WILEY-VCH Verlag GmbH & Co. KGaA, Weinheim. Impact of backbone regiochemistry.[55] (e) Equilibrium molecular structures and SOMOs of the charged (i.e., anionic) species for RR and RI oligomers ($n = 5$). Calculations are at the UωB97X-D/6-311G* level for the RR and at the BS-UωB97X-D/6-311G* level for the RI. (f) Electrical conductivity of RR- and RI-P(NDI2OD-T2) bulk films as a function of TDAE exposure time and N-DMBI molar ratio. Adapted with permission, 2019 American Chemical Society.

In devotions of enhancing conductivity and thermoelectric performance of n-type polymer by tailoring the molecular D-A character and steric conformation, several other works are noted. Wang and Takiyama investigated the impact of backbone orientation by synthesizing two pNB derivates, as shown in Fig. 6(a).[37] The differences between these three molecular are the –R function groups branched on naphtodithiophenediimide (NDTI) and the connection units between NDTI and bithiopheneimide (BTI). On the unit of pNB-Tz, the NDTI and BTI are connected by two –Tz function groups, on pNB-TzDP, the side chains of NDTIs are further modified from 2-decyltetradecyls to 3-decylpentadecyls. Such modifications lead to a more linear backbone conformation of Pnb-Tz and pNB-TzDP than original pNB. The following GIWAXS patterns elucidated a shift of polymer backbone orientation, from face-on of pNB to edge-on of pNB-Tz and then to bimodal of pNB-TzDP. The π–π stacking distance and intensity were strengthened, moreover, the interchain aligned side chains offered larger free space than pNB in pNB-Tz and pNB-TzDP, implying better doping ability, which was proved by following experiments. After doped with N-DMBI, for pNB-TzDP, the σ reached to 11.6 S/cm, over 1000 times higher than pNB and 100 times higher than pNB-Tz (Fig. 6(c)), this may attributed to better accommodation to dopant, which originally resulted from larger side chain volume and a lower E_a. The power factor of pNB-TzDP was also several folds higher than that of other two counterparts, estimated as 53.4 μW·m^{-1}·K^{-2}. To understand these large variations in properties, UV-vis-NIR

spectroscopy was applied. Since the branching point of side chain may affect the π-conjugation effect, the pNB-TzDP was superior to two counterparts because it is branched at a further position on the backbone, weakened the hinderance of dopant mixing together with polymer chain. Several new absorptions were found, which were attributed to some polaronic changes on the polymer backbones after doping. With stronger and more intensive polaronic effect, the pNB-TzDP eventually gained higher charge carrier density, doping level and other properties. In a specially designed GIWAXS test, the micro aggregational structures of polymers in varied dopant ratios were investigated. The packing distance of pNB-TzDP was almost the same as pristine sample, even after doped at 50 mol%, the lamellar packing distance only occurred slight rise, from 22.1 Å to 22.6 Å. Furthermore, the π–π stacking distance also remained unchanged, indicating that dopants are likely to stay in amorphous area, such as among side chains, the schematic cartoon is illustrated in Fig. 6(d). These results proved that lamellar orientation, chain conformation, stacking distance and polaron induced conductive charge carrier pathways are essential to achieve high performances.

Through donor engineering, Yang *et al.* reported a novel D-A polymer with high charge carrier mobility,[56] they synthesized two D-A polymers: PDPH and PDPF, replacing H^+ atoms with F^+, the electron-withdrawing ability of donor moiety was reinforced. Though these two pristine monomers showed competitive charge carrier mobility and other properties, PDPF could be better doped by n-type dopant and more stable stacking structure after doping. Doped with N-DMBI, when the doping level increased, the Coulomb traps began to affect the polarons, thus the charge carrier mobility improved. PDPF reached its highest conductivity at 7% N-DMBI content as 1.30 ± 0.20 S/cm, while the doped PDPH can only reach three grades of magnitude lower while with even heavier doping level. PDPF could also maintain the performance of conductivity longer than PDPH. The Seebeck factor of PDPF was -235 μV/K, 5 times higher than that of PDPH, as well as grades of magnitude higher in power factors than other references. In coming GIWAXS and AFM scans, intrinsic PDPH and PDPF were similar in lamellar and π–π stacking structure, but after doping process, PDPF displayed good miscibility with N-DMBI and larger crystalized area, the π–π stacking distance remained almost the same. These all suggested better chain stacking and packing.

The idea of tailoring steric demand and donor–acceptor character can be also found in many recent researches. Moreover, some investigations also focused on more detailed micro structure of single building block. Wang and Fazzi *et al.* discussed the impact of backbone regiochemistry on the properties of n-doped D-A polymers.[55] In Wang and Fazzi's research about P(NDI2OD-T2), they investigated the difference of conductivity, charge density and polaronic structure derived from regioirregular (RI) and regioregular (RR) chain comformations. Unlike the conventional homopolymers such as P3HT as a counterpart in the paper, the more twisted RI-P(NDI2OD-T2) with less charge carriers and rougher morphorlogy shows higher doped electrical conductivity. After investigated by implementing by several methods of characterization and DFT calculation, these outcomes are attributed to the RI structure has made P(NDI2OD-T2) to be more tolerable to disorder. RI-P(NDI2OD-T2) can also doped heavier than RR-P(NDI2OD-T2) (Fig. 6(f)). In EPR test, RI structure possess more paramagnetic species, which is considered to be the contribution of different chain structure, polaronic structure and spin density calculated by DFT (Fig. 6(e)). Moreover, though the spatial microstructures of both P(NDI2OD-T2) seem to be different, it appears that the intrachain sterics are not affected, thus RI-P(NDI2OD-T2) may show similar LUMO energy and chain comformation.

6. Summary and outlook

In this review, a brief introduction of n-type OTEs on the materials side is given. We first illustrated the working principles of OTEs, and what it takes to build high performance OTE device, that is a delicate balance between electrical conductivity, thermal conductivity and Seebeck coefficient, as well as equivalent p- and n-components when building into a commercially valuable thermoelectric generator. The relatively low doping efficiency and thus low electrical conductivity of n-type OTEs are one of the key issues to be solved at current stage. We have examined some of the latest answers in this area, including the efforts of lowering the LUMO levels of n-type polymers, weakening the D-A characteristics of classical conjugated semiconducting polymers, increasing the miscibility of polymer matrix and the dopants, and most importantly improving the planarity and rigidity of the polymer backbone. That can be done by utilizing ladder type polymers with tough lock between repeating units, or by tuning the steric conformation with modified functional groups and substituters. The combination of the key points mentioned above seems to give the best performance n-type OTEs to date.

After years of developing and many record-breaking works published, the structure–property relationship of n-type thermoelectric polymers is becoming more evident and a readily available knowledge. Recently, new reports like regulating the thermo-conductivity of the doped system, or employing mixed ionic-electronic TE effects have emerged, giving high n-type ZT over 0.3 and 0.2,[57,58] respectively, which may infuse the field with new vitality.

Acknowledgements

Project supported by the Fundamental Research Funds for the Central Universities, China (Grant No. 21D110637), the National Natural Science Foundation of China (Grant

No. 52173156), the Science and Technology Commission of Shanghai Municipality, China (Grant No. 20JC1414900), and the Chinese Academy of Sciences (Faculty Consultation and Evaluation Project 2020-ZW07-A-017).

References

[1] Wang Y, Yang L, Shi X, Shi X, Chen L, Dargusch M S, Zou J and Chen Z 2019 *Adv. Mater.* **31** 1807916

[2] Gao W, Ota H, Kiriya D, Takei K and Javey A 2019 *Acc. Chem. Res.* **52** 523

[3] Wang S, Xu J, Wang W, Wang G J N, Rastak R, Molina-Lopez F, Chung J W, Niu S, Feig V R, Lopez J, Lei T, Kwon S K, Kim Y, Foudeh A M, Ehrlich A, Gasperini A, Yun Y, Murmann B, Tok J B H and Bao Z 2018 *Nature* **555** 83

[4] Rogers J A, Someya T and Huang Y 2010 *Science* **327** 1603

[5] Shi Q, Sun J, Hou C, Li Y, Zhang Q and Wang H 2019 *Adv. Fiber Mater.* **1** 3

[6] Yang J, Li X L, Zhou J W, Wang B and Cheng J L 2020 *Chin. J. Polym. Sci.* **38** 403

[7] Hasan M N, Wahid H, Nayan N and Mohamed Ali M S 2020 *Int. J. Energy Res.* **44** 6170

[8] Beretta D, Neophytou N, Hodges J M, Kanatzidis M G, Narducci D, Martin-Gonzalez M, Beekman M, Balke B, Cerretti G, Tremel W, Zevalkink A, Hofmann A I, Müller C, Dörling B, Campoy-Quiles M and Caironi M 2019 *Mater. Sci. Eng. R Reports* **138** 100501

[9] Russ B, Glaudell A, Urban J J, Chabinyc M L and Segalman R A 2016 *Nat. Rev. Mater.* **1** 16050

[10] Yang Y and Gao W 2019 *Chem. Soc. Rev.* **48** 1465

[11] Liu Y, Pharr M and Salvatore G A 2017 *ACS Nano* **11** 9614

[12] Cheng T, Zhang Y, Lai W Y and Huang W 2015 *Adv. Mater.* **27** 3349

[13] Hong Y, Cheng X L, Liu G J, Hong D S, He S S, Wang B J, Sun X M and Peng H S 2019 *Chin. J. Polym. Sci.* **37** 737

[14] Lu Y, Wang J Y and Pei J 2019 *Chem. Mater.* **31** 6412

[15] Sheng P, Sun Y, Jiao F, Di C, Xu W and Zhu D 2014 *Synth. Met.* **193** 1

[16] Sun Y, Qiu L, Tang L, Geng H, Wang H, Zhang F, Huang D, Xu W, Yue P, Guan Y, Jiao F, Sun Y, Tang D, Di C, Yi Y and Zhu D 2016 *Adv. Mater.* **28** 3351

[17] Zhang B, Sun J, Katz H E, Fang F and Opila R L 2010 *ACS Appl. Mater. Interfaces* **2** 3170

[18] Sarabia-Riquelme R, Craddock J, Morris E A, Eaton D, Andrews R, Anthony J and Weisenberger M C 2017 *Synth. Met.* **225** 86

[19] Sato R, Kiyota Y, Kadoya T, Kawamoto T and Mori T 2016 *RSC Adv.* **6** 41040

[20] Zuo G, Li Z, Wang E and Kemerink M 2018 *Adv. Electron. Mater.* **4** 1700501

[21] Kroon R, Mengistie D A, Kiefer D, Hynynen J, Ryan J D, Yu L and Müller C 2016 *Chem. Soc. Rev.* **45** 6147

[22] Liang Z, Choi H H, Luo X, Liu T, Abtahi A, Ramasamy U S, Hitron J A, Baustert K N, Hempel J L, Boehm A M, Ansary A, Strachan D R, Mei J, Risko C, Podzorov V and Graham K R 2021 *Nat. Mater.* **20** 518

[23] Zhu J, Tang D, Wang W, Liu J, Holub K W and Yang R 2010 *J. Appl. Phys.* **108** 94315

[24] Schmidt A J, Cheaito R and Chiesa M 2009 *Rev. Sci. Instrum.* **80** 94901

[25] Schwarze M, Gaul C, Scholz R, Bussolotti F, Hofacker A, Schellhammer K S, Nell B, Naab B D, Bao Z, Spoltore D, Vandewal K, Widmer J, Kera S, Ueno N, Ortmann F and Leo K 2019 *Nat. Mater.* **18** 242

[26] Lüssem B, Keum C M, Kasemann D, Naab B, Bao Z and Leo K 2016 *Chem. Rev.* **116** 13714

[27] Lu Y, Yu Z, Un H, Yao Z, You H, Jin W, Li L, Wang Z, Dong B, Barlow S, Longhi E, Di C, Zhu D, Wang J, Silva C, Marder S R and Pei J 2021 *Adv. Mater.* **33** 2005946

[28] Bubnova O, Khan Z U, Wang H, Braun S, Evans D R, Fabretto M, Hojati-Talemi P, Dagnelund D, Arlin J B, Geerts Y H, Desbief S, Breiby D W, Andreasen J W, Lazzaroni R, Chen W M, Zozoulenko I, Fahlman M, Murphy P J, Berggren M and Crispin X 2014 *Nat. Mater.* **13** 190

[29] Vijayakumar V, Durand P, Zeng H, Untilova V, Herrmann L, Algayer P, Leclerc N and Brinkmann M 2020 *J. Mater. Chem. C* **8** 16470

[30] Shalini V, Navaneethan M, Harish S, Archana J, Ponnusamy S, Ikeda H and Hayakawa Y 2019 *Appl. Surf. Sci.* **493** 1350

[31] Gueye M N, Carella A, Faure-Vincent J, Demadrille R and Simonato J P 2020 *Prog. Mater. Sci.* **108** 100616

[32] Park E B, Yoo J S, Park J Y, Park Y W, Akagi K and Shirakawa H 1995 *Synth. Met.* **69** 61

[33] Lu B, Yuk H, Lin S, Jian N, Qu K, Xu J and Zhao X 2019 *Nat. Commun.* **10** 1043

[34] Wang S, Ruoko T P, Wang G, Riera-Galindo S, Hultmark S, Puttisong Y, Moro F, Yan H, Chen W M, Berggren M, Müller C and Fabiano S 2020 *ACS Appl. Mater. Interfaces* **12** 53003

[35] Wang S, Sun H, Ail U, Vagin M, Persson P O A, Andreasen J W, Thiel W, Berggren M, Crispin X, Fazzi D and Fabiano S 2016 *Adv. Mater.* **28** 10764

[36] Schlitz R A, Brunetti F G, Glaudell A M, Miller P L, Brady M A, Takacs C J, Hawker C J and Chabinyc M L 2014 *Adv. Mater.* **26** 2825

[37] Wang Y and Takimiya K 2020 *Adv. Mater.* **32** 2002060

[38] Liu J, Ye G, Potgieser H G O, Koopmans M, Sami S, Nugraha M I, Villalva D R, Sun H, Dong J, Yang X, Qiu X, Yao C, Portale G, Fabiano S, Anthopoulos T D, Baran D, Havenith R W A, Chiechi R C and Koster L J A 2021 *Adv. Mater.* **33** 2006694

[39] Shi K, Zhang F, Di C A, Yan T W, Zou Y, Zhou X, Zhu D, Wang J Y and Pei J 2015 *J. Am. Chem. Soc.* **137** 6979

[40] Un H I, Gregory S A, Mohapatra S K, Xiong M, Longhi E, Lu Y, Rigin S, Jhulki S, Yang C Y, Timofeeva T V, Wang J Y, Yee S K, Barlow S, Marder S R and Pei J 2019 *Adv. Energy Mater.* **9** 1900817

[41] Ding Y, Yang C, Huang C, Lu Y, Yao Z, Pan C, Wang J and Pei J 2021 *Angew. Chemie* **133** 5880

[42] Lu Y, Yu Z Di, Liu Y, Ding Y F, Yang C Y, Yao Z F, Wang Z Y, You H Y, Cheng X F, Tang B, Wang J Y and Pei J 2020 *J. Am. Chem. Soc.* **142** 15340

[43] Lu Y, Yu Z Di, Un H I, Yao Z F, You H Y, Jin W, Li L, Wang Z Y, Dong B W, Barlow S, Longhi E, Di C an, Zhu D, Wang J Y, Silva C, Marder S R and Pei J 2021 *Adv. Mater.* **33** 2005946

[44] Hwang S, Potscavage W J, Yang Y S, Park I S, Matsushima T and Adachi C 2016 *Phys. Chem. Chem. Phys.* **18** 29199

[45] Kotadiya N B, Mondal A, Blom P W M, Andrienko D and Wetzelaer G J A H 2019 *Nat. Mater.* **18** 1182

[46] Yan X, Xiong M, Li J T, Zhang S, Ahmad Z, Lu Y, Wang Z Y, Yao Z F, Wang J Y, Gu X and Lei T 2019 *J. Am. Chem. Soc.* **141** 20215

[47] Kiefer D, Giovannitti A, Sun H, Biskup T, Hofmann A, Koopmans M, Cendra C, Weber S, Anton Koster L J, Olsson E, Rivnay J, Fabiano S, McCulloch I and Müller C 2018 *ACS Energy Lett.* **3** 278

[48] Fazzi D, Fabiano S, Ruoko T P, Meerholz K and Negri F 2019 *J. Mater. Chem. C* **7** 12876

[49] Lu Y, Yu Z Di, Zhang R Z, Yao Z F, You H Y, Jiang L, Un H I, Dong B W, Xiong M, Wang J Y and Pei J 2019 *Angew. Chemie-Int. Ed.* **58** 11390

[50] Wang S, Sun H, Erdmann T, Wang G, Fazzi D, Lappan U, Puttisong Y, Chen Z, Berggren M, Crispin X, Kiriy A, Voit B, Marks T J, Fabiano S and Facchetti A 2018 *Adv. Mater.* **30** 1801898

[51] Intemann J J, Yao K, Yip H L, Xu Y X, Li Y X, Liang P W, Ding F Z, Li X and Jen A K Y 2013 *Chem. Mater.* **25** 3188

[52] Xu L, Selin V, Zhuk A, Ankner J F and Sukhishvili S A 2013 *ACS Macro Lett.* **2** 865

[53] Chang J F, Clark J, Zhao N, Sirringhaus H, Breiby D W, Andreasen J W, Nielsen M M, Giles M, Heeney M and McCulloch I 2006 *Phys. Rev. B* **74** 115318

[54] Liu J, Ye G, Zee B van der, Dong J, Qiu X, Liu Y, Portale G, Chiechi R C and Koster L J A 2018 *Adv. Mater.* **30** 1804290

[55] Wang S, Fazzi D, Puttisong Y, Jafari M J, Chen Z, Ederth T, Andreasen J W, Chen W M, Facchetti A and Fabiano S 2019 *Chem. Mater.* **31** 3395

[56] Yang C Y, Jin W L, Wang J, Ding Y F, Nong S, Shi K, Lu Y, Dai Y Z, Zhuang F D, Lei T, Di C A, Zhu D, Wang J Y and Pei J 2018 *Adv. Mater.* **30** 1802850

[57] Liu J, van der Zee B, Alessandri R, Sami S, Dong J, Nugraha M I, Barker A J, Rousseva S, Qiu L, Qiu X, Klasen N, Chiechi R C, Baran D, Caironi M, Anthopoulos T D, Portale G, Havenith R W A, Marrink S J, Hummelen J C and Koster L J A 2020 *Nat. Commun.* **11** 5694

[58] Jiang Q, Sun H, Zhao D, Zhang F, Hu D, Jiao F, Qin L, Linseis V, Fabiano S, Crispin X, Ma Y and Cao Y 2020 *Adv. Mater.* **32** 2002752